A Sparse Topic Relaxion and Group Clustering Model for Hyperspectral Unmixing

Qiqi Zhu, *Member, IEEE*, Linlin Wang, *Graduate Student Member, IEEE*, Wen Zeng, Qingfeng Guan, and Zhen Hu

***Abstract*—Hyperspectral unmixing (HU) has been a hot research topic in the field of hyperspectral remote sensing. In recent years, the employment of the probabilistic topic model to acquire the latent topics of hyperspectral images has been an effective method for spectral unmixing. However, such methods fail to fully exploit the potential of topic models in uncovering image semantics, and they need extra sparsity constraints, which greatly increases the complexity of the model. To solve these problems, a sparse topic relaxion and group clustering model for HU (STRGC) is proposed. In STRGC, the sparse prior constraints implied by the sparse topic model are introduced, which means that the sparse characteristics of the model are used to capture the semantic representation of the spectrum. Through the relaxation of the model, the possible spectral representations of ground features can be obtained, and this further alleviates the influence caused by endmember variability on the accuracy of the unmixing process. Then, fuzzy clustering is used to locate the position of the endmember quickly and accurately. Furthermore, unmixing models with different characteristics are united to alleviate the ill-posed nature of the model, thereby improving the fractional abundance. Experimental results obtained with one simulated dataset and three well-known real hyperspectral datasets confirm the effectiveness and advantages of the proposed method.**

***Index Terms*—Abundance, endmember, group clustering, hyperspectral unmixing (HU), sparse topic relaxion.**

I. Introduction

With the development of remote sensing sensors, the wealth of spectral information of hyperspectral images (HSIs) has opened new perspectives in many fields, such as environmental monitoring, precision agriculture, forestry monitoring and mineral exploration [1]. However, due to the mixed effects of the ground surface and the low spatial resolution of the sensor, a single pixel may involve multiple spectral features, leading to the phenomenon of "mixed pixel" [2], [3]. In this case, hyperspectral unmixing (HU) is one of the crucial steps for the deep development of HSIs [4]. Specifically, HU is aimed at identifying the spectral signatures of the pure constituent spectra in the HSIs (called endmembers) and corresponding proportion of each endmember (known as abundances) in each image pixel [5].

Spectral unmixing can be summarized into the next categories [6]: 1) Geometrical, 2) sparse regression, 3) statistical, and 4) deep learning-based methods. Geometrical approaches assume that linearly mixed vectors are located in a positive cone or in a simplex set. In this way, vertex component analysis (VCA) uses convex geometry rules to efficiently perform unmixing tasks [7]. The determination of the fractional abundances can then be handled by least-squares-based methods, such as fully constrained least squares (FCLS) [8]. Specifically, the combination of using VCA to extract endmembers and using FCLS to estimate abundances is called VCA-FCLS in unmixing [9]. However, these methods are mainly suitable for situations where the examined image contains pure pixels and satisfies the noise-free condition. Thus, although geometrical models have high computational efficiency, they often fail to capture highly mixed spectral features [10]. Sparse regression methods treat the unmixing process as a linear regression problem on a given spectral library. The input image is expressed as a combination of spectral signatures by the semisupervised procedure. For these approaches, a spectral library of image features needs to be constructed, and the regression process incurs a high-computational cost [11], [12]. Statistical approaches determine the endmember and abundance parameters by using parameter estimation techniques, thus expressing them in a probability distribution. The core of such an approach is to assume that the endmembers of each pixel come from a sample following a certain probability distribution [13], [14]. Regarding deep learning methods, such as radial-basis function (RBF) neural network and backward propagation (BP) neural network have been used to estimate the abundances of mixed pixels [15], [16]. In this case, each training sample of the neural network is composed of a mixed pixel and its corresponding abundance fractions, and the weight values of these samples are adjusted through supervised training. Although good results can be obtained, such methods usually need a large number of training samples and multiple parameters must be adjusted [17]–[19]. In addition, this kind of methods cannot meet the abundance sum-to-one constraint (ASC) and abundance nonnegative constraint (ANC), which usually cause their unmixing results unacceptable.

Broadly speaking, the aforementioned methods have been shown to be effective under specific conditions. Specifically,

Manuscript received January 28, 2021; revised March 14, 2021; accepted March 19, 2021. Date of publication March 30, 2021; date of current version April 21, 2021. This work was supported in part by the National Natural Science Foundation of China under Grant 41901306, in part by the Open Research Project of The Hubei Key Laboratory of Intelligent Geo-Information Processing under Grant KLIGIP-2019A02, in part by a Grant from State Key Laboratory of Resources and Environmental Information System, and in part by Special Fund for Foundation and Frontier of Applications of Wuhan under Grant 2018010401011293. *(Corresponding author: Zhen Hu.)*

The authors are with the High-performance Spatial Computational Intelligence Lab, School of Geography and Information Engineering, China University of Geosciences, Wuhan 430078, China (e-mail: zhuqq@cug.edu.cn; wll@cug.edu.cn; zengwen@cug.edu.cn; guanqf@cug.edu.cn; huzhenstars@163.com).

Digital Object Identifier 10.1109/JSTARS.2021.3069574

the sparse regression and statistical-based methods have been proven to achieve better results in highly mixed scenes. However, sparse unmixing, as a semisupervised method, is difficult to find a stable, optimal, and unique solution, and the spectral library should be obtained in advance. In contrast, the statistical approaches hold the advantage of not requiring a prior spectral library. Considering the problem of the endmember variability, statistical methods are usually taken as solutions to model the distribution of endmembers. It assumes that the endmember of each pixel is generated by sampling a certain probability distribution. The current popular methods based on statistical model includes Gaussian mixture model (GMM) [20], [21]. Researches have shown that an image can be explained by representative topics, which contribute a lot to the semantic understanding of the image, such as scene classification [22], image annotation [23], etc. Additionally, the probabilistic topic model (PTM) has shown great potential in the task of HU due to its property of effectively dealing with multiple tasks by expressing a high-level semantic understanding of data. In this case, HSIs can be viewed as a data cube, where each pixel is represented by a vector that indicates its spectral reflectance at various wavelengths. This reflectance vector is most likely a mixture. By analyzing the semantic information of the image and converting the spectrum of each pixel into a probability distribution, the corresponding spectral decomposition result is obtained.

In order to avoid overfitting caused by complex models, sparsity can be used to reduce the solution space and the number of parameters that need to be inferred [24]. It is consistent with the fact that most pixels are mixed only by a few features in the scene for HSI. In fact, the performance of an unmixing model can be significantly improved when considering the sparsity assumption. To avoid the problem of dense topics being used for modeling the images, sparsity has been regarded as an appropriate constraint for a topic model utilized to cope with HSIs. In other words, adding sparsity constraints to the unmixing model helps estimate spectral features and fractional abundances. This also provides room for improvement in the study of topic-based HU models [27]. In detail, Wang *et al*. first tackled the unmixing task as a latent topic-based method and proposed the sparsity-constrained probabilistic latent semantic analysis (SC-PLSA), and this algorithm obtained relatively high efficiency in HU. However, this model which introduces sparse constraints by selecting regularization terms with auxiliary parameters may cause problems with large-scale datasets. Fernandez-Beltran *et al*. developed a new PLSA-based model in which two sparsity factors are introduced into the topic and image to combine sparsity. However, the introduced sparsity factors are only fixed constants artificially preset, and the model shows high model complexity and time consumption [24]–[26].

In topic-based approaches, the fully sparse topic model (FSTM) mines the sparse topics of documents with linear convergence. FSTM is a simple but efficient method for highly complex scenes [28]. More specifically, it utilizes the ability of flexible implicit semantic mining and the Frank–Wolf algorithm's sparse reasoning to estimate endmembers and abundances quickly. However, the sparse characteristics of the FSTM may cause a lack of semantic information in cases where there are more topics than actual endmembers. Existing studies have shown that VCA-FCLS can achieve high-computational efficiency, accuracy, and flexibility when the image contains pure pixels or satisfies the noise-free condition [7].

Motivated by the abovementioned problems, in this work, a novel and effective method named the sparse topic relaxion and group clustering model for HU (STRGC) is proposed. In STRGC, flexible implicit semantic mining and Frank–Wolf algorithm's sparse reasoning are used to estimate the initial endmembers and abundances. Specifically, we relax the topics to approximate the possible representations of endmembers for solving the problem of endmember variability [29]. Then, fuzzy C-means (FCM) clustering is employed when the number of topics is more than the number of actual endmembers [30], [31]. Moreover, considering the respective characteristics of the FSTM and VCA-FCLS with respect to HU, a weighted strategy is adopted for the model to achieve more accurate endmembers and abundances. Our novelty is that we propose a framework that flexibly applies the powerful semantic mining capabilities and sparsity constraints of the sparse topic model to HU. Although previous studies have used topic models to extract the semantic information of images for HU, these models [such as PLSA and latent Dirichlet allocation (LDA)] need to add additional sparsity constraints to adapt to HU scenarios, and this greatly increases the model complexity and unmixing difficulty. In this study, the natural sparse features of the sparse topic model are applied to HU, and the flexible implicit semantic mining function of the sparse topic model and the sparse reasoning ability of the Frank–Wolf algorithm are used to extract the hidden endmembers and estimate abundances. In addition, the experimental comparison involving the model relaxation and clustering strategy proves that this method can effectively alleviate the impact of endmember variability, thereby further showing that our proposed framework can solve the incompatibility issues encountered when directly applying topic models to unmixing.

The main contributions of this study are as follows.

1) To effectively express the discriminative semantic information in HSIs and reduce the complexity of the unmixing model, the sparse topic relaxation model (STRM) is introduced as an unsupervised unmixing strategy for obtaining the initial endmembers and fractional abundances. Then, the semantic representations extracted from the initial spectral space are used to alleviate the ill-posed characteristic of the HU problem. Note that the STRM does not require extra sparsity constraints and thus is model-independent. Based on the implicit sparsity constraints of the STRM, the framework can reduce the solution space and the number of parameters to be extracted and further improve the unmixing rate.
2) To avoid endmember uncertainty and the lack of abundances caused by sparsity, FCM clustering is used when the number of actual endmembers is less than the number of topics. Moreover, the endmembers are determined through the relaxation and clustering of the model, and this can effectively alleviate the influence of endmember variability on unmixing.
3) Considering that the STRM has good flexibility and accuracy with respect to solving endmember variability and highly complex scenes and because VCA-FCLS can

achieve high-computational efficiency when the examined image contains pure pixels and satisfies the noise-free condition, the STRGC framework is proposed to obtain improved unmixing results. Moreover, the proposed framework can obtain endmembers and abundances without spectral libraries and thus is unsupervised.

Comprehensive evaluations on one simulated dataset and three well-known real hyperspectral imagery datasets, as well as comparisons with some popular HU methods available in the existing literature, verify the effectiveness and superiority of the proposed methods.

The rest of the article is arranged as follows. Section II introduces the related work. Section III discusses details about the proposed STRGC framework for HSI unmixing. Section IV is devoted to experiments with synthetic and real datasets. Finally, Section V concludes this article.

II. Background

STRGC is closely related to the topic model and other classic models, e.g., the FSTM, VCA-FCLS, and FCM. In this section, we briefly introduce related unmixing models.

A. Classic Topic Model and FSTM

Classic topic models include PLSA and LDA [32]–[34]. In 2001, Hofmann proposed the PLSA model. For PLSA, the terms W, Z, and D denote the visual word, topic, and document, respectively. However, because PLSA lacks a probability function for describing the document, the number of model parameters increases linearly with the size of the documents.

In 2003, the LDA model was proposed; it adds a Dirichlet distribution to the topic mixture θ based on the PLSA model. LDA provides a probability function for the discrete implicit topics in PLSA and is regarded as a complete PTM. However, the latent semantics discovered from documents by LDA are often dense, thereby yielding a large amount of redundant information and requiring additional storage space. Some studies have tried to reduce the complexity of the model by encoding a spike-and-slap distribution or utilizing regularization to induce sparse topics [35]–[37]. However, they still have some limitations: When dealing with large-scale datasets, auxiliary parameters related to the regularization terms require model selection, and they cannot directly weigh the sparsity of solutions with time and quality [28].

In 2012, as a simplified variant of PLSA and LDA, the FSTM was proposed. FSTM uses an implicit sparse prior to process documents instead of Dirichlet priors and extra sparsity constraints. In particular, it cancels the endowment of the Dirichlet distribution in LDA. When deleting the observation variable associated with each document, the FSTM can also be regarded as a variant of PLSA. Fig. 1 represents the probabilistic graphical model of the FSTM. Existing research shows that compared with other models, the FSTM has obviously superior performance in terms of the learning and inference times, the model complexity, and the sparsity of the implicit representations of documents. In more detail, the inference algorithm converges to optimal solutions at a linear rate, and the learning algorithm has low complexity, which means that there exists an approximately dimensionless method for performing dimensionality reduction (DR). Moreover, it provides an effective approach for directly weighing the sparsity of the obtained solutions with quality and time [28].

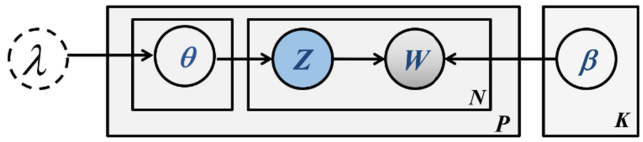

Fig. 1. Probabilistic graphical model of the FSTM.

B. FCM Clustering

As an unsupervised technique, FCM clustering has been successfully used for clustering, feature analysis, and classifier design in fields such as image segmentation, target recognition, medical imaging, and spectral unmixing. Specifically, the FCM algorithm can be used to analyze the distances between multiple input datasets. Then, clusters are generated based on the distances between the datasets, and a cluster center is generated for each cluster. In addition, datasets are clustered into n clusters, and each dataset is associated with its corresponding cluster. Each dataset and its corresponding cluster have a high rate of affiliation and are as far away from other clusters as possible [38]–[40]. The FCM clusters the obtained samples into a class C with an iterative optimization approach that minimizes the objective function. For each pixel, the fuzzy membership degrees in the FCM obtained from all classes sum to unity.

C. VCA-FCLS

In the existing research, the HU problem based on linear mixing model (LMM) can be divided into endmember estimation and abundance inversion, which are then processed separately. A variety of geometrical HU methods have been applied to obtain endmembers. In this case, the VCA algorithm iterates the projection data in a direction orthogonal to the subspace spanned by the determined endmembers. The new endmember corresponds to the most extreme projection. The algorithm is repeated until all endmembers are obtained. It is worth noting that VCA assumes that there are pure pixels in the dataset, but this may not be sufficient for most scenes. On the other hand, the inversion of fractional abundances can be handled by least-squares-based approaches. In addition, the combination of VCA for endmember extraction and FCLS for abundance inversion can be used to obtain the final unmixing results [8], [9].

III. Adaptive Weighting Framework With Sparse Topic Relaxion and Group Clustering

To fully consider the applicability of the unmixing model and effectively utilize the semantic information in images, the STRGC framework is proposed for HSI unmixing. This is an ensemble approach that combines spatial, spectral, and semantic

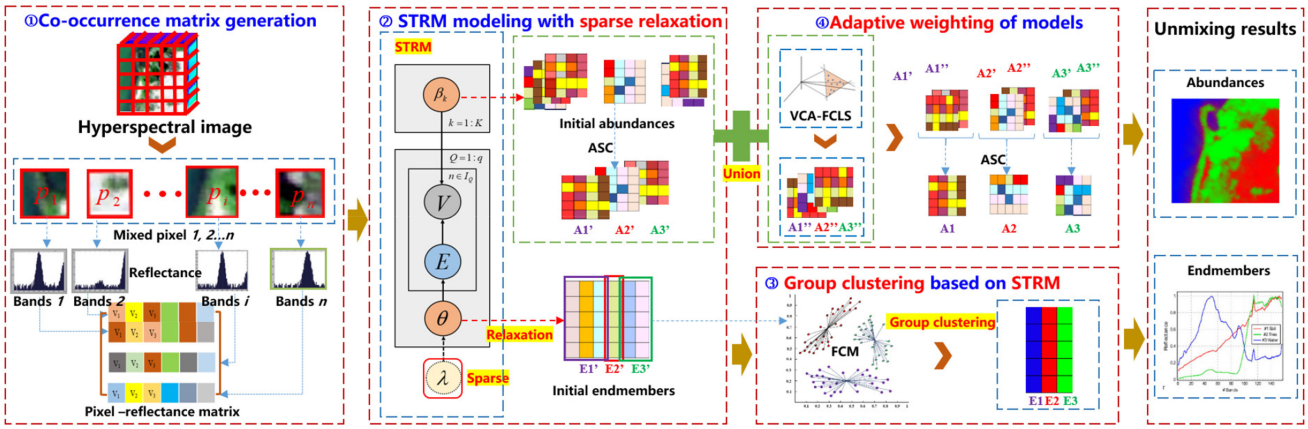

Fig. 2. Flowchart for HU based on the STRGC framework. A pixel reflectance matrix is first generated and then input into the proposed STRM model with sparse relaxation to obtain the initial abundances and initial endmembers. The initial endmembers are clustered according to the FCM algorithm to obtain the final endmembers, whose corresponding abundances are clustered into the same group and added to obtain the abundances based on the STRM. Finally, the final abundances are obtained by the adaptive weighting of the abundances based on VCA-FCLS and the abundances based on the STRM.

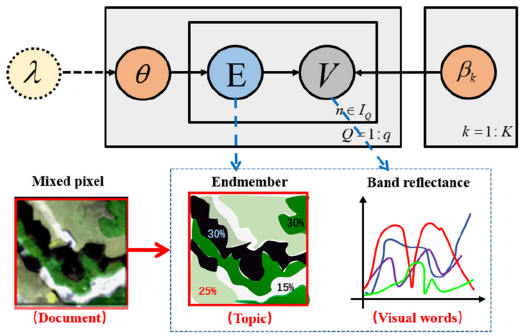

Fig. 3. Correspondences between HU and the STRM.

features. For STRGC, four tasks must be addressed: 1) Cooccurrence matrix generation, 2) STRM modeling with sparse relaxation, 3) group clustering based on the STRM, and 4) adaptive model weighting. The overall flow chart for HU based on the STRGC framework is presented in Fig. 2. In the flow chart, $E1'$, $E2'$, and $E3'$ represent the initial endmembers based on the STRM. $A1'$, $A2'$, $A3'$, and $A1''$, $A2''$, $A3''$ are the obtained abundances using the STRM and VCA-FCLS, respectively.

A. Cooccurrence Matrix Generation

Through the sparse relaxation strategy, the STRM model based on the FSTM is introduced. When the STRM is applied to HSI unmixing, the relationships between their respective terminologies are described in Fig. 3. A corpus corresponds to a HSI, and a document is equivalent to one pixel Q in the image. Topics depict the endmembers E. Words are considered spectral bands V, and the word count in each document is considered equivalent to the reflectance of a pixel band.

Before integrating the vectors, the uniform method is utilized to split the whole HSI into pixel blocks. The rich spectral information in HSIs provides data support for feature classification and target recognition. The massive bands of each pixel can correspond to the visual words. The different reflectance of bands is converted into 1D histograms based on multiple pixels. Then, a statistical analysis is performed for each band reflection, and a pixel-band cooccurrence matrix is generated. In this case, each row of the matrix represents a pixel, and each element denotes the value of the spectral reflectance in each band.

B. STRM Modeling With Sparse Relaxation

The index for the N local patches is represented as j, the index for the Q pixels is expressed as i, and the index for the topics is represented as k. The STRM assumes that a mixed pixel can be represented with K endmembers, denoted by $\beta_{1,\ldots}\beta_K$. The unmixing process of the STRM for the HSIs is shown as follows.

1) For every pixel, a K-dimensional topic proportion θ is randomly selected within a reasonable range.
2) For each band in pixel Q , a latent endmember E_k is selected for each pixel conditional on the probability $p(E_k|Q_i) = \theta_k$ within a reasonable range, and then a spectral reflectance V_j is selected with probability . The probability $p(V_j|Q_i)$ between spectral reflectance and pixel Q_i can be described as follows:

$$P(V_j|Q_i) = \sum_{k=1}^{K} p(V_j|E_k)p(E_k|Q_i). \tag{1}$$

It is worth noting that despite being a simplified variant, it has been confirmed that the STRM contains an implicit prior of the topic distribution, and the density function is expressed as (2). This interesting property of "implicit modeling" enables the STRM to converge to the best solution at a linear rate. In this study, the STRM is used for modeling the endmembers with sparsity

$$P(\theta|\lambda) \propto \exp(-\lambda. \parallel \theta\|_0). \tag{2}$$

To obtain sparse implicit endmembers, the STRM uses the sparsity of the original pixels and endmember proportions. In other words, learning endmembers is equivalent to multiplying the new representation θ of the HSI with the original representation Q. The inference and learning tasks of the STRM algorithm are shown in Fig. 4.

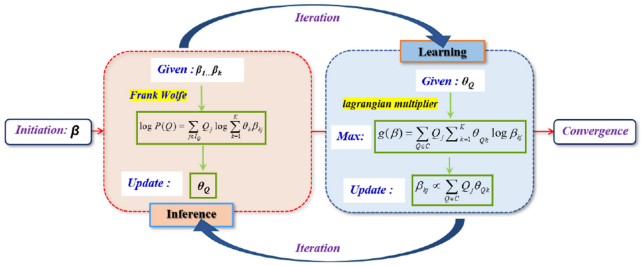

Fig. 4. Inference and learning tasks of the STRM algorithm.

The inference task is reconstructed as a concave maximization problem on the simplex of endmembers. Specifically, the inference task can be described as the problem of seeking θ to maximize the likelihood of Q. Moreover, the probability that spectral reflectance V_j appears in a given pixel Q can be denoted by

$$P(V_j|Q) = \sum_{k=1}^{K} P(V_j|E_k) \cdot P(E_k|Q) = \sum_{k=1}^{K} \theta_k \beta_{kj}. \tag{3}$$

Therefore, the log likelihood of Q can be described by

$$\log P(Q) = \log \prod_{j \in I_Q} P(V_j|Q)^{Q_i} = \sum_{j \in I_Q} Q_j \log \sum_{k=1}^{K} \theta_k \beta_{kj}. \tag{4}$$

Denote $x_j = \sum_{k=1}^{K} \theta_k \beta_{kj}$, which represents the convex combination of at most $L+1$ vertices of the simplex $\Delta = \mathrm{conv}(\beta_1, \ldots, \beta_k)$ after L iterations, and let $x = (x_1, \ldots, x_V)^t = \sum_{k=1}^{K} \theta_k \beta_k$. This implies that $\sum_k \theta_k = 1, \theta_k \geq 0$. The log likelihood of Q can be expressed as

$$\log P(Q) = \sum_{j \in I_Q} Q_j \log x_j. \tag{5}$$

We infer the proportion θ_k of latent endmembers in each pixel Q by maximizing the objective function. Note that simply limiting the number of iterations in the Frank–Wolfe algorithm can directly control the sparsity of the endmember proportions θ.

The learning task of the STRM is to learn all endmembers $\beta = (\beta_1, \ldots, \beta_k)$ when given an image I. The EM algorithm is used to iteratively learn the model. In this case, the E-step and M-step are repeated until convergence is achieved. Specifically, for the E-step, an inference is performed for every pixel Q of image I; for the M-step, the likelihood of I is maximized with respect to β. Taking the Lagrange function into account and forcing its derivatives to be 0, this learning process can update all endmembers by only performing simple calculations according to

$$\beta_{kj} \propto \sum_{Q \in I} Q_j \theta_{Qk}. \tag{6}$$

C. Group Clustering Based on STRM

For real scenes, one spectrum does not completely correspond to one material in an HSI. This phenomenon means that the endmembers can change along with the pixels. To avoid the detrimental unmixing effect caused by endmember variability, we take advantage of the sparsity of the STRM to relax the topics and obtain the possible forms of each endmember. In other words, the number of topics is greater than the actual number of endmembers when using the STRM for unmixing. In this case, FCM clustering is introduced to extract endmembers. The class membership values, which are output by the FCM algorithm, may be interpreted as degrees of sharing or posterior probabilities. This allows analysts to adjust the fuzziness of the output, which is attractive for decomposing the class composition of the pixels. Note also that these values are relative measures of the category membership strength, so the calculation is performed for all classifications. Suppose the sample set $S = \{s_1, s_2, \ldots, s_N\}$, where $S_j = \{j = 1, 2, \ldots, N\}$ represents the D-dimensional feature vector in FCM clustering. The FCM algorithm minimizes the objective function [denoted as (7)] by using an iterative optimization process; then, these samples are clustered into C classes

$$J = \sum_{i=1}^{C} \sum_{j=1}^{N} \mu_{ij}^{m} \parallel s_j - v_i \parallel^2. \tag{7}$$

The constraints are as

$$\mu_{ij} \in [0,1]; 0 < \sum_{j=1}^{N} \mu_{ij} < N, \forall i; \sum_{i=1}^{C} \mu_{ij} = 1 \forall j \tag{8}$$

where μ_{ij} represents the fuzzy membership of pixel s_j in the ith cluster; m is the fuzziness parameter; C denotes the number of classes; v_i represents the ith cluster center; and $m > 1$ denotes the weighted index of each fuzzy membership used to control the fuzziness of the analysis. The clustering centers and the membership degrees are obtained in an unsupervised clustering manner in the fuzzy model, where the clustering centers refer to endmembers. In this case, the endmember generation process can be described as follows: First, based on the sparse reasoning ability and fast convergence characteristics of the STRM, initial possible endmembers are mined from HSIs. Then, according to the FCM algorithm, the improved endmembers that are expressed as cluster centers are chosen by deriving the strength of membership of every endmember in the corresponding class. Correspondingly, we can group the corresponding abundances for the same feature according to the division of endmembers and follow the ASC to obtain improved abundances.

D. Enhancing the Unmixing Results By Utilizing Adaptive Model Weighting

For the task of improving the endmembers and abundances, the STRM and VCA-FCLS are united effectively. Based on the ability of flexible implicit semantic mining and the Frank–Wolf algorithm's sparse reasoning in the STRM, endmembers and abundances can be quickly estimated. However, the sparse topics obtained only by the STRM may lack representative semantic features. Moreover, the existing unmixing researches have shown that different models will exhibit different performances according to their HU characteristics. For real HSIs, the endmembers may have multiple representations, whose shapes

Algorithm 1: STRGC for Hyperspectral Unmixing.

Input: Dataset Y.
Output: Endmembers E, abundances A.
Step 1. /∗ ***Cooccurrence matrix M for initialization*** ∗/
1. **Generate** A.
Step 2. /∗***STRM for unmixing according to*** Fig. 4∗/
2. Infer the proportion θ_k.
3. Learn all topics β by using an EM scheme.
repeat
a) E-step: Update θ_k by (4) and (5).
b) M-step: Update β_{kj} via (6).
until convergence
Step 3. /∗***FCM for unmixing***∗/
4. Generate E and A' by (7).
Step 4. /∗ *Adaptive weighting of models* ∗/
5. Obtain A'' via VCA-FCLS.
6. Generate A.

cannot be represented by a single distribution. In this case, the STRM can approximate any distribution found in the library and has high accuracy and flexibility in solving the endmember variability problem. VCA-FCLS has a higher unmixing effect when pure pixels exist in the HSI. Based on this, abundances of the same features obtained from the STRM and VCA-FCLS are united by appropriate weights to acquire the final abundances. In more detail, for simple images, the abundance of VCA-FCLS has a greater weight, which is adaptively adjusted between 0.65–0.9. In contrast, for complex images, the STRM is given more weight.

Finally, the pseudocode of the proposed STRGC algorithm is summarized in Algorithm 1.

IV. Experiments and Analysis

A. Experimental Settings

In this section, four different hyperspectral datasets are considered in our experiments: One simulated dataset, called Simu, and three real HSI datasets, i.e., the Samson dataset, Jasper dataset, and Urban dataset, as shown in Fig. 5.

To evaluate the unmixing performances of the proposed models, two quantitative metrics are used in our experiments [41]–[44]: the spectral angle distance (SAD), defined as in (9), and the root-mean-square error (RMSE), as shown in (10)

$$\mathrm{SAD}(\hat{V}, V) = \frac{1}{K}\sum_{i}^{K} \arccos \frac{\hat{V}_i \cdot V_i}{\| \hat{V}_i \| \, \| V_i \|} \tag{9}$$

$$\mathrm{RMSE}(\hat{M}, M) = \sqrt{\frac{1}{R \cdot C}\sum_{i}^{R}\sum_{j}^{C} \left(\hat{M}_{i,j} - M_{i,j}\right)^2} \tag{10}$$

where K indicates the number of endmembers. $\hat{V}$ and V represent the estimated endmembers and the corresponding ground truth, respectively. R and C are the sizes of the input images. $\hat{M}$ and M act as the estimated abundances and the corresponding ground truth, respectively. To evaluate the performances of the proposed methods, the experimental results

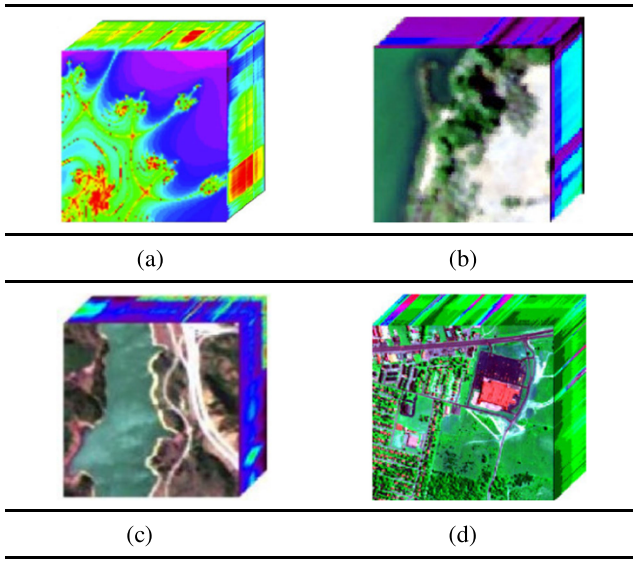

Fig. 5. HSIs used in the experiments. (a) Simu. (b) Samson. (c) Jasper. (d) Urban.

obtained with the conventional GMM [20], VCA-FCLS [7], minimum volume simplex analysis (MVSA) [9], and the FSTM [28] are provided for comparison purposes. In addition, we also provide the test results obtained with NMF-based methods, NMF-sp [45], and collaborative nonnegative matrix factorization (CNMF) [46], and topic-based methods, PLSA [33], PLSA-sp [22], which introduces a sparsity constraint over the documents, and LDA [32], as shown in the latest papers [23]. To further illustrate the effectiveness of the proposed method for complex datasets, the results of some recent methods, a deep autoencoder network (DAEN) [16], a stacked nonnegative sparse autoencoder (SNSA) [18], a deep autoencoder unmixing (DAEU) [47], and dyadic cyclic descent optimization (DCD) [48], are shown in the results of the Jasper and Urban datasets [16]–[19].

B. Simulated Experiment: Simu Dataset

The Simu dataset is generated by the simulation procedure proposed in [49], as shown in Fig. 5(a); it has a size of 100 × 100 pixels and contains 221 channels. It consists of nine endmembers chosen from the geological survey (USGS) spectral library: Kaolinite 1, Dumortierite, Nontronite, Alunite, Sphene, Pyrophyllite, Halloysite, Muscovite, and Kaolinite 9. The corresponding abundance results are obtained by a Gaussian filter with k-means clustering, and the filter is also subject to nonnegative and additive constraints [50]. Research has shown that the signal-to-noise ratio (SNR) observed in real hyperspectral imaging instruments is increasing. Therefore, the consideration of a low SNR value should not be taken as an indication of the true parameter value of the current hyperspectral imaging state [49]. In our experiments, three levels of noise are added to the Simu dataset, i.e., SNRs of 30, 50, and 70, as follows:

$$\mathrm{SNR} = 10\log_{10}\frac{E\left[X^T X\right]}{E\left[n^T n\right]} \tag{11}$$

TABLE I
ENDMEMBER SAD ASSESSMENT FOR THE SIMU DATASET

Datasets	E	Spectral Angle Distance - SAD									
		Non-topic-based methods					Topic-based methods				
		VCA-FCLS	MVSA	NMF-sp	CNMF	GMM	LDA	PLSA	PLSA-sp	FSTM	STRM
Simu (no noise)	9	**0.0029**	0.0005	0.2011	0.0007	0.0790	0.3959	0.2477	0.1438	0.1316	0.1159
Simu (SNR 30)	9	**0.0253**	0.0976	0.2220	0.0718	0.0802	0.4525	0.3082	0.2123	0.1309	0.1255
Simu (SNR 50)	9	**0.0039**	0.0288	0.2097	0.0130	0.0664	0.4267	0.2838	0.1795	0.1326	0.1247
Simu (SNR 70)	9	**0.0030**	0.0028	0.2040	0.0015	0.0640	0.4113	0.2578	0.1584	0.1323	0.1254

Note that the displayed values are the averages of the experiment, with the best results in bold.

TABLE II
ABUNDANCE RMSE ASSESSMENT FOR THE SIMU DATASET

Datasets	E	Root Mean Squared Error– RMSE										
		Non-topic-based methods					Topic-based methods					
		VCA-FCLS	MVSA	NMF-sp	CNMF	GMM	LDA	PLSA	PLSA-sp	FSTM	STRM	STRGC
Simu (no noise)	9	0.0082	0.2182	0.1701	0.0015	0.3066	0.1499	0.1586	0.1568	0.2515	0.2479	**0.0082**
Simu (SNR 30)	9	0.0449	0.2271	0.1683	0.0968	0.2879	0.1714	0.1903	0.1909	0.2498	0.2469	**0.0449**
Simu (SNR 50)	9	0.0098	0.2237	0.1701	0.0142	0.3194	0.1616	0.1835	0.1723	0.2543	0.2248	**0.0098**
Simu (SNR 70)	9	0.0082	0.2227	0.1701	0.0022	0.3332	0.1557	0.1809	0.1584	0.2534	0.2343	**0.0082**

Note that the displayed values are the averages of the experiment, with the best results in bold.

where $E[\cdot]$ is the expectation operator, and X, n denote the original signal and the corresponding noise, respectively.

The quantitative assessments are provided in Tables I and II for the Simu dataset. In addition to the quantitative evaluation presented by the SAD and RMSE metrics, the qualitative evaluations provided by the abundance maps are also shown. Fig. 6 shows the abundance fractions of STRGC and the ground-truth abundances.

It can be seen from the above table that for the SAD, VCA-FCLS achieves the best results. The main reason for this is that the noncomplex features of the Simu dataset make it easy for pure pixels to appear. However, due to mixing phenomena, spatial resolutions, and other considerations, pure spectral components are almost nonexistent in real hyperspectral scenes. Moreover, in topic model-based methods, the effect of the FSTM is significantly greater than those of PLSA and LDA. Among them, the STRM improved by sparse relaxation is better than PLSA-sp with sparsity constraints. Regarding the improvement of the model, the result of the STRM based on sparse relaxation is better than that of the FSTM. For the RMSE, compared with other methods, the geometric method can obtain strong abundance results, but the proposed adaptive weighted framework can also achieve good accuracy. Moreover, the accuracy of the STRM improved by the sparse relaxation strategy is effectively improved in terms of both the SAD and RMSE. As depicted in Fig. 6, the comparison results for abundance indicate that the proposed STRGC can obtain almost the same effect as the ground truth, thereby demonstrating the effectiveness of the proposed methods.

C. Real Data Experiment 1: Samson Dataset

The Samson dataset [51], as shown in Fig. 5(b), has 156 channels and a size of 952 × 952 pixels; it is used for the HU experiment. A region of size 95 × 95 is selected from the (252, 332)th pixel in the original image. Soil, trees, and water are chosen as the references for three endmembers. Fig. 7 shows the obtained abundances by the above methods and the ground-truth abundances for the Samson dataset. The comparison between the endmembers and abundances obtained with the various methods is provided in Tables III and IV.

Similar to the Simu dataset, Samson is simple, and there are numerous pure pixels in the dataset. When considering the SAD metric, the geometrical-based method yields good results in terms of the estimated endmembers, which agree with the characteristics of the data. However, the proposed STRGC achieves a more accurate RMSE result than that of VCA-FCLS. In addition, the accuracy of the STRM using the sparse relaxation strategy is effectively improved with respect to both endmembers and abundances. The results of STRGC agree with the ground truth in the abundance maps.

D. Real Data Experiment 2: Jasper Dataset

Jasper is a popular hyperspectral dataset [51]–[53]. It contains 224 bands, and the spectral resolution is 9.46 nm. Moreover, to avoid atmospheric effects, bands 1–3, 108–112, 154–166, and 220–224 are removed (198 channels remained). As shown in Fig. 5(c), considering the high complexity of the image, a 100 × 100 × 198 subimage cropped from the original image is used in

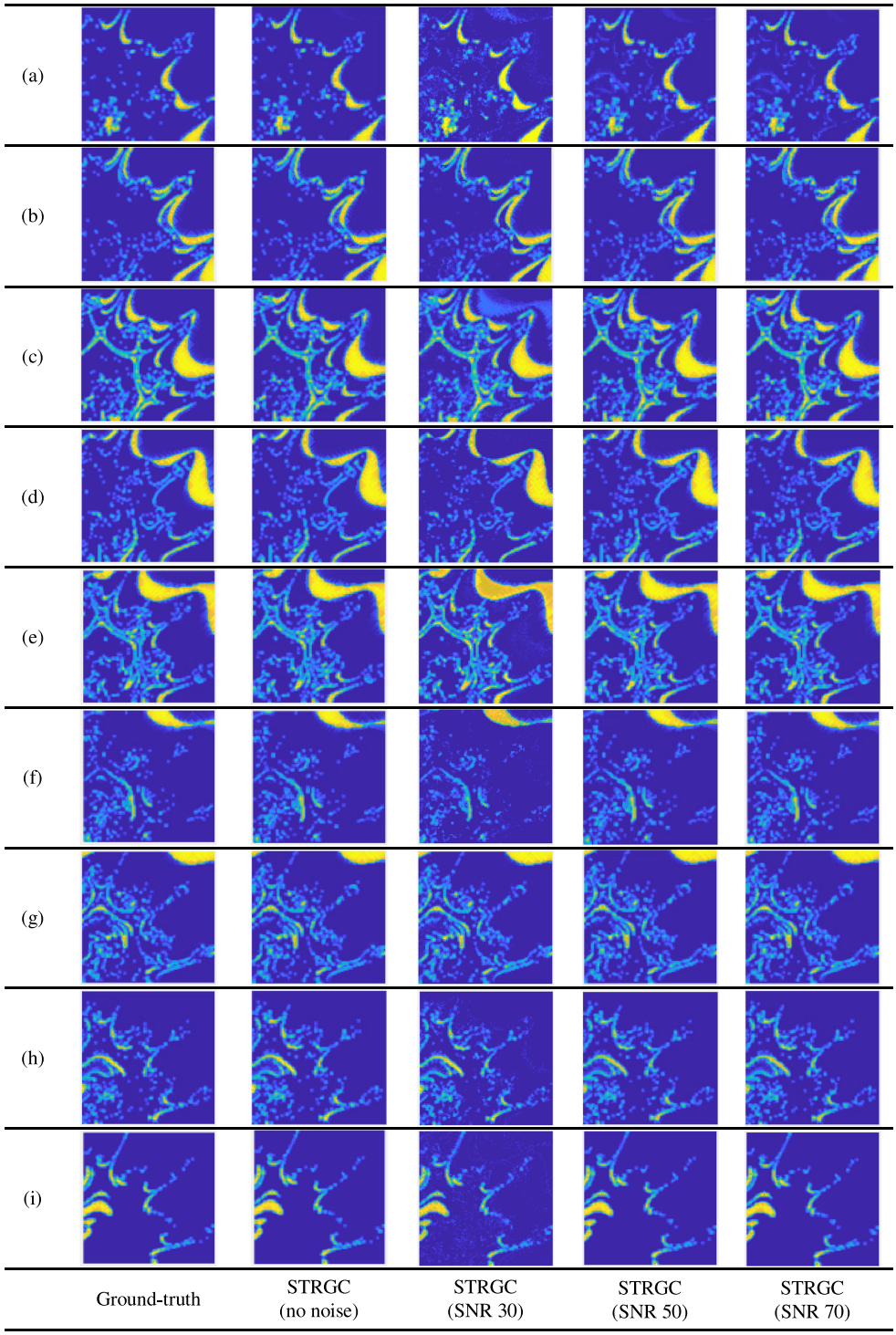

Fig. 6. Ground-truth abundances and the STRGC abundances for Simu. (a) Kaolinite 1. (b) Dumortierite. (c) Nontronite. (d) Alunite. (e) Sphene. (f) Pyrophilite. (g) Halloysite. (h) Muscovite. (i) Kaolinite 9.

our experiments. The image has the following four endmembers: Tree, water, soil, and road. Tables V and VI are the results for the endmembers and abundances, respectively. In Fig. 8, the corresponding abundances and the ground-truth abundances are shown.

From the results reported in Tables V and VI, we can see that the proposed methods achieve competitive results relative to those of other methods. Specifically, among the topic model-based methods, the FSTM is better than PLSA and LDA, where the STRM is better than PLSA-sp. After relaxation and clustering are performed, the accuracy of the STRM is better than that of the FSTM. In general, STRGC is significantly better than using the STRM and VCA-FCLS alone, and it has the highest unmixing accuracy. In comparison with the ground-truth

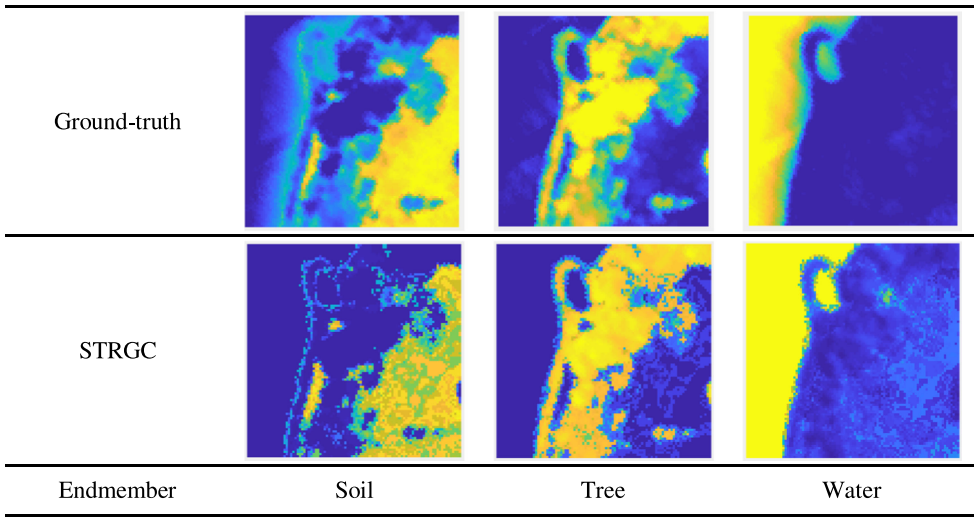

Fig. 7. Ground-truth abundances and the STRGC abundances for Samson.

TABLE III
ENDMEMBER SAD ASSESSMENT FOR THE SAMSON DATASET

Datasets	E	Spectral Angle Distance - SAD									
		Non-topic-based methods					Topic-based methods				
		VCA-FCLS	MVSA	NMF-sp	CNMF	GMM	LDA	PLSA	PLSA-sp	FSTM	STRM
Samson	3	**0.0713**	0.1632	0.1310	0.1186	0.1154	0.3495	0.1927	0.1264	0.2046	0.1969

Note that the displayed values are the averages of the experiment, with the best results in bold.

TABLE IV
ABUNDANCE RMSE ASSESSMENT FOR THE SAMSON DATASET

Datasets	E	Root Mean Squared Error– RMSE										
		Non-topic-based methods					Topic-based methods					
		VCA-FCLS	MVSA	NMF-sp	CNMF	GMM	LDA	PLSA	PLSA-sp	FSTM	STRM	STRGC
Samson	3	0.3146	0.3799	0.1382	**0.1233**	0.2126	0.2773	0.1951	0.1268	0.2322	0.1606	0.1544

Note that the displayed values are the averages of the experiment, with the best results in bold.

TABLE V
ENDMEMBER SAD ASSESSMENT FOR THE JASPER DATASET

Datasets	E	Spectral Angle Distance - SAD												
		Non-topic-based methods								Topic-based methods				
		VCA-FCLS	MVSA	NMF-sp	CNMF	GMM	DAEN	SNSA	DCD	LDA	PLSA	PLSA-sp	FSTM	STRM
Jasper	4	0.1672	0.2842	0.2570	0.2935	0.2315	0.1680	0.1508	0.1413	0.3639	0.3041	0.3007	0.1943	**0.1400**

Note that the displayed values are the averages of the experiment, with the best results in bold.

TABLE VI
ABUNDANCE RMSE ASSESSMENT FOR THE JASPER DATASET

Datasets	E	Root Mean Squared Error– RMSE										
		Non-topic-based methods					Topic-based methods					
		VCA-FCLS	MVSA	NMF-sp	CNMF	GMM	LDA	PLSA	PLSA-sp	FSTM	STRM	STRGC
Jasper	4	0.1515	0.3880	0.1562	0.2630	0.1539	0.2773	0.1951	0.2036	0.1489	0.1284	**0.1057**

Note that the displayed values are the averages of the experiment, with the best results in bold.

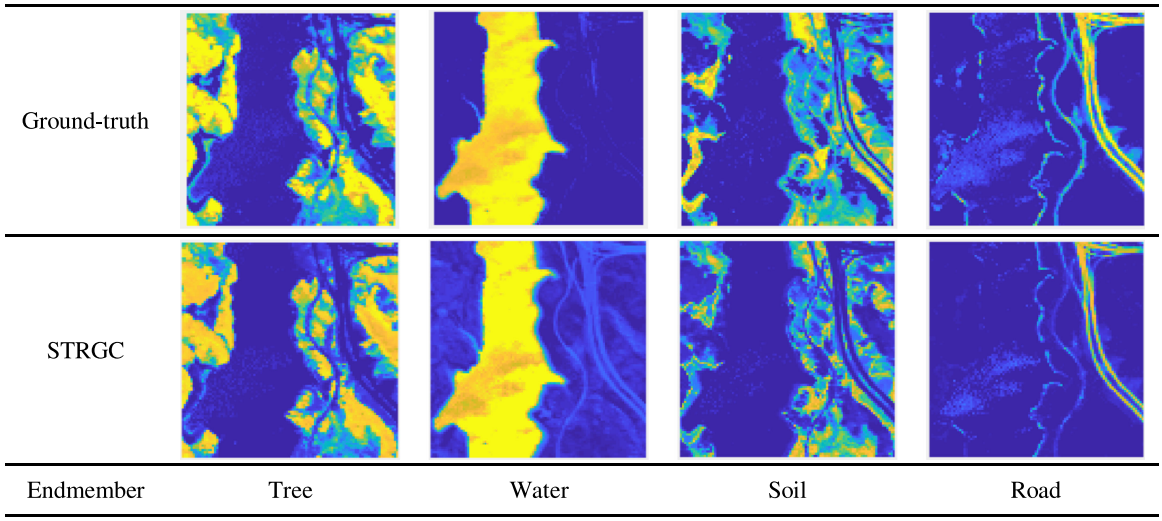

Fig. 8. Ground-truth abundances and the STRGC abundances for Jasper.

TABLE VII
ENDMEMBER SAD ASSESSMENT FOR THE URBAN DATASET

Datasets	E	Spectral Angle Distance - SAD												
		Non-topic-based methods								Topic-based methods				
		VCA-FCLS	NMF-sp	CNMF	GMM	DAEN	SNSA	DCD	DAEU	LDA	PLSA	PLSA-sp	FSTM	STRM
Urban	4	0.2941	0.2395	0.2686	0.4081	0.4304	0.4194	0.4500	0.1456	0.4091	0.3324	0.3091	0.1710	**0.1230**

Note that the displayed values are the averages of the experiment, with the best results in bold.

TABLE VIII
ABUNDANCE RMSE ASSESSMENT FOR THE URBAN DATASET

Datasets	E	Root Mean Squared Error– RMSE										
		Non-topic-based methods					Topic-based methods					
		VCA-FCLS	MVSA	NMF-sp	CNMF	GMM	LDA	PLSA	PLSA-sp	FSTM	STRM	STRGC
Urban	4	0.3134	0.3044	0.1284	0.2307	0.3071	0.2124	0.1748	0.1547	0.1967	0.1381	**0.1192**

Note that the displayed values are the averages of the experiment, with the best results in bold.

abundance maps, the proposed STRGC can achieve almost the same result for each feature.

E. Real Data Experiment 3: Urban Dataset

The Urban dataset [51]–[53], as shown in Fig. 5(d), has a size of 307 × 307 pixels and 210 bands covering the 400–2500-nm wavelength range. During preprocessing, some noisy and corrupted bands are removed (162 bands remain). The ground truth contains four endmembers: Asphalt, grass, tree, and roof. Tables VII and VIII list the quantitative results of the endmembers and abundances, respectively, for urban areas. Fig. 9 shows the corresponding abundance results and the ground-truth abundances.

As can be seen from Tables VII and VIII, the proposed approach can obtain high-precision results with respect to both endmembers and abundances. Compared to the geometric methods, VCA and MVSA, statistical methods, NMF-sp, CNMF, and GMM, deep learning-based methods, DAEN, SNSA, DCD, and DAEU, and traditional topic-based methods, LDA, PLSA, and PLSA-sp, the proposed methods can achieve higher accuracy in terms of both SAD and RMSE. Moreover, the accuracy of the STRM improved by sparse relaxation is significantly higher than that of the FSTM. The results further illustrate the advantages of the proposed approaches for unmixing with complex images. The abundances estimated from STRGC are good matches with the corresponding abundances in the ground truth.

Overall, the proposed methods are experimentally verified to perform well on both the qualitative assessment and the quantitative evaluation. Although the geometric methods exhibit good performance in the extraction of endmembers for simple datasets, due to mixing phenomena, spatial resolutions and other factors, pure spectral components are almost nonexistent in real hyperspectral scenes. Their estimations of abundances are certainly not as effective as those of endmembers. In contrast, the proposed approaches are proven to exhibit better unmixing capabilities for real complex images. From the data complexity analysis, for simulated data and the relatively simple Samson

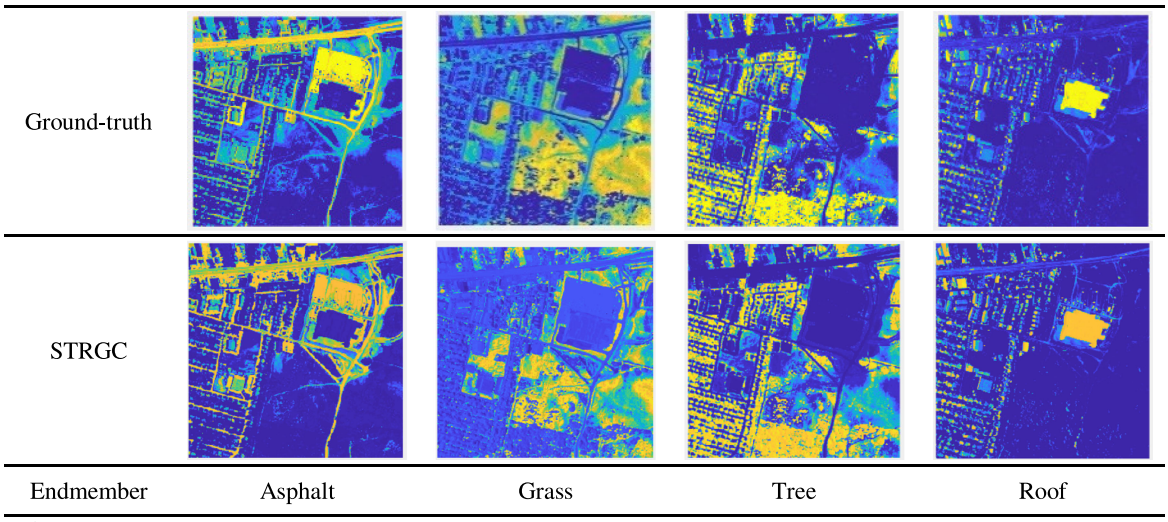

Fig. 9. Ground-truth abundances and the STRGC abundances for Urban.

data, the accuracy of STRGC is significantly improved through the adaptive weighting strategy of VCA-FCLS and the STRM. For highly complex Jasper images, the accuracy of STRGC is the best in terms of both SAD and RMSE. For the large and complex Urban images, the proposed methods have obvious advantages in both SAD and RMSE, indicating the applicability of the proposed strategy to complex scenes. The accuracy of STRGC is significantly better than those of the geometric methods, deep learning-based methods, and other statistical methods. From the comparison of different unmixing methods, the FSTM is better than the traditional PLSA and LDA approaches, and the improved STRM using relaxation and clustering is better than PLSA-sp for unmixing based on topic models. On the whole, the proposed method is able to retrieve stable endmember and abundance estimates for both simple datasets and complex datasets, and this further reflects the robustness of the proposed STRGC in actual applications. The advantages are remarkable, especially for problems with relatively complex images. In addition, it can be seen that the improved STRM is better than the FSTM in terms of both SAD and RMSE, and this reflects the effectiveness of the proposed relaxation strategy. On the other hand, for all images in the experiment, the abundance maps obtained by STRGC and the real abundance maps are relatively consistent, and this also confirms the rationality and effectiveness of the proposed methods.

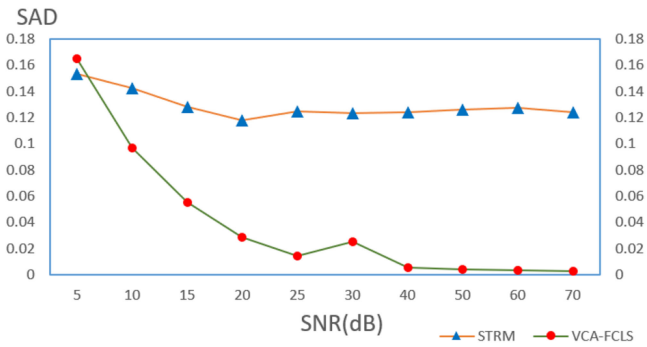

Fig. 10. SAD comparison between the algorithms with Gaussian noise.

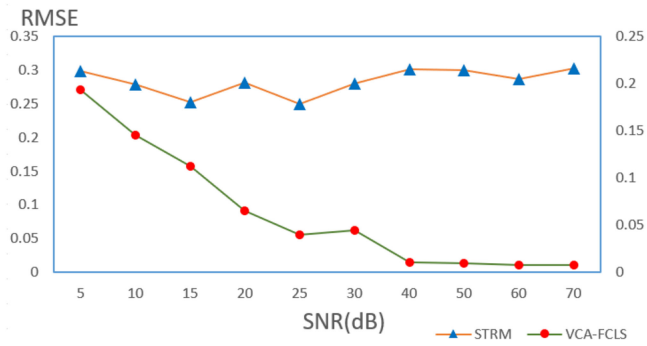

Fig. 11. RMSE comparison between the algorithms with Gaussian noise.

V. Discussion

A. Analysis of Robustness to Noise

Considering that in real hyperspectral data production scenarios, images are usually affected by many different types of disturbances and image corrections that also introduce some noise, we conduct this experiment to compare and analyze the performances of the various algorithms. In this experiment, the Simu dataset is polluted by different levels of white Gaussian noise, where the SNR $= \{5, 15, 20, 25, 30, 40, 50, 60, 70$ dB$\}$.

Figs. 10 and 11 show the SAD and RMSE comparisons between the different algorithms with Gaussian noise, respectively.

As seen in Figs. 10 and 11, the VCA-FCLS algorithm generally outperforms the proposed STRM algorithm in terms of both SAD and RMSE. However, as the SNR increases (e.g., SNR $\geq$ 5 dB), the VCA-FCLS algorithm displays a large fluctuation. In contrast, the proposed STRM seems to be largely unaffected by the added noise and presents a relatively stable and robust performance under different noise conditions.

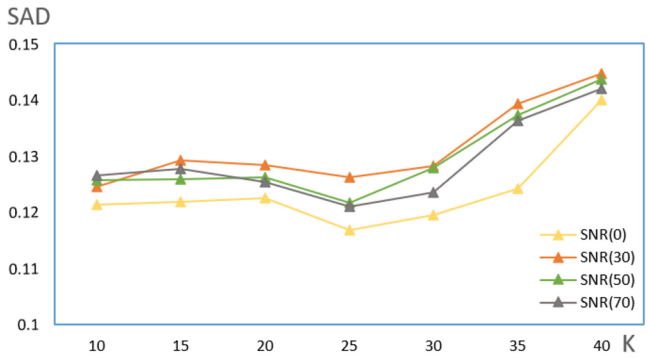

Fig. 12. Sensitivity analysis in relation to the topic number K for Simu dataset.

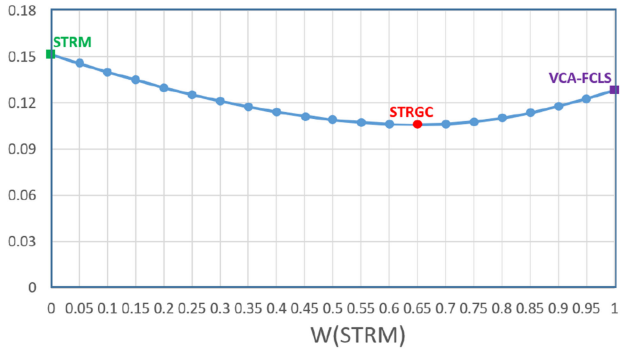

Fig. 13. RMSE of STRGC under different weight settings.

TABLE IX
COMPUTATIONAL TIMES OF DIFFERENT METHODS

Datasets	E	Times (seconds)				
		VCA-FCLS	NMF-sp	CNMF	STRM	STRGC
Samson	3	2.32	57.99	26.79	24.34	26.66
Jasper	4	2.7	38.02	19.81	7.67	10.37
Urban	4	7.98	73.32	191.33	129.73	137.71

TABLE X
REASONABILITY COMPARISON OF COMBINING SPARSE TOPIC MODEL AND GROUP FCM

Datasets	E	SAD		RMSE	
		FSTM	**FSTM +FCM**	FSTM	**FSTM +FCM**
Samson	3	0.2046	**0.1969**	0.2322	**0.1606**
Jasper	4	0.1943	**0.1400**	0.1489	**0.1284**
Urban	4	0.1710	**0.1230**	0.1967	**0.1381**

B. Sensitivity Analysis in Relation to the Topic Number K

In order to investigate the effect of relaxion of the latent topic on inaccurate endmember extraction, we tested the Simu dataset with the actual number of endmembers being 9. The topic number K of Simu datasets with different SNRs were set to 10,15,20,25,30, respectively. As can be seen from Fig. 12, when the number of topics is less than 30, it has less influence on the endmember estimation. That is, the proposed method is relatively stable as the topic number K varies within a reasonable range. Once the number of topics over a reasonable range increases, the accuracy gradually decreases.

C. Comparison of Computational Times

To test the time complexity of the proposed algorithm, we present the experimental running times of the various algorithms on real datasets. Table IX summarizes the calculation times required for the VCA-FCLS, NMF-sp, CNMF, STRM, and STRGC methods on the test image.

Overall, VCA-FCLS takes the least amount of time due to its simplicity, and the topic-based method has a faster unmixing rate than the NMF-based method. For simple Samson data and Jasper data, the proposed STRM requires relatively little time. For complex Urban images, the running times of different algorithms are increased significantly, and the time required by the proposed STRM is second only to that of CNMF.

D. Analysis of the Adaptive Weighting Unified Framework

To analyze the contributions made by the different components of the proposed framework and taking the characteristics of the test image into account, we select Jasper images for an experiment. In this experiment, the weight W of the abundances produced by the STRM is adaptively adjusted from 0 to 1. Fig. 13 shows the changes in accuracy yielded with different weights.

As shown in Fig. 13, compared with those of the original STRM and VCA-FCLS, the RMSE of the STRGC model after performing adaptive weighting is significantly improved. Because the accuracy of the STRM is higher than that of VCA-FCLS, the proposed framework achieves the optimal result when the STRM occupies a larger weight (approximately 0.65).

E. Reasonability of Sparse Topic Relaxion and Group Clustering

To analyze the reasonability of combining sparse topic model and group FCM for HU, ablation studies on different datasets are implemented. SAD and RMSE of the Samson dataset, Jasper dataset, and the Urban dataset are reported in Table X. As shown in Table X, the endmember estimation and abundance inversion of the proposed FSTM+FCM performs better in the three datasets compared to FSTM by the topic relaxion and group clustering strategies, which confirms the reasonability of combining sparse topic model and group FCM for HU.

VI. CONCLUSION

In this study, an efficient unmixing framework called STRGC based on a topic model is proposed for HSI unmixing. In STRGC, the topic model is used to model a given image by the statistics related to the spectral reflectance of each pixel to obtain additional semantic information. In this case, the sparse inference ability and features of fast convergence of the STRM are utilized to mine hidden endmembers and estimate fractional abundances in HSIs. To extract the endmembers in a highly efficient way, we relax the topics by the sparsity of the STRM to obtain the possible spectral representations of each endmember, thereby alleviating a series of problems caused by endmember variability in HU. Then, FCM clustering is adopted to further extract endmembers and estimate abundances. With regard to the improvements in the abundances, the adaptive weighting of VCA-FCLS and the STRM further utilizes their respective characteristics in unmixing and improves accuracy. This study

shows that the proposed STRGC has better performance than the traditional topic model in finding high-quality semantic representations from HSIs and has a lower model complexity. It achieves the best SAD and RMSE scores on all real datasets except for the Samson dataset, and this demonstrates the unmixing advantages of STRGC in highly complex scenes. In future work, we plan to further exploit the proposed framework by considering the automatic determination of the number of endmembers to improve the practicality of the proposed method.

REFERENCES

[1] J. M. Bioucas-Dias, A. Plaza, G. Camps-Valls, P. Scheunders, N. Nasrabadi, and J. Chanussot, "Hyperspectral remote sensing data analysis and future challenges," *IEEE Geosci. Remote Sens. Mag.*, vol. 1, no. 2, pp. 6–36, Jun. 2013.

[2] A. Plaza, Q. Du, J. M. Bioucas-Dias, X. Jia, and F. A. Kruse, "Foreword to the special issue on spectral unmixing of remotely sensed data," *IEEE Trans. Geosci. Remote Sens.*, vol. 49, no. 11, pp. 4103–4110, Nov. 2011.

[3] G. A. Shawand and H. Burke, "Spectral imaging for remote sensing," *Lincoln Lab. J.*, vol. 14, no. 1, pp. 3–28, 2003.

[4] W.-K. Ma *et al.*, "A signal processing perspective on hyperspectral unmixing," *IEEE Signal Process. Mag,* vol. 31, no. 1, pp. 67–81, Jan. 2014.

[5] N. Keshava and J. F. Mustard, "Spectral unmixing," *IEEE Signal Process. Mag.*, vol. 19, no. 1, pp. 44–57, Jan. 2002.

[6] J. M. Bioucas-Dias *et al.*, "Hyperspectral unmixing overview: Geometrical, statistical, and sparse regression-based approaches," *IEEE J. Sel. Topics Appl. Earth Observ. Remote Sens.*, vol. 5, no. 2, pp. 354–379, Apr. 2012.

[7] J. M. P. Nascimento and J. M. Bioucas-Dias, "Vertex component analysis: A fast algorithm to unmix hyperspectral data," *IEEE Trans. Geosci. Remote Sens.*, vol. 43, no. 4, pp. 898–910, Apr. 2005.

[8] D. C. Heinz and C.-I. Chang, "Fully constrained least squares linear spectral mixture analysis method for material quantification in hyperspectral imagery," *IEEE Trans. Geosci. Remote Sens.*, vol. 39, no. 3, pp. 529–545, Mar. 2001.

[9] J. Li, A. Agathos, D. Zaharie, J. M. Bioucas-Dias, A. Plaza, and X. Li, "Minimum volume simplex analysis: A fast algorithm for linear hyperspectral unmixing," *IEEE Trans. Geosci. Remote Sens.*, vol. 53, no. 9, pp. 5067–5082, Sep. 2015.

[10] T.-H. Chan, W.-K. Ma, A. Ambikapathi, and C.-Y. Chi, "A simplex volume maximization framework for hyperspectral endmember extraction," *IEEE Trans. Geosci. Remote Sens.*, vol. 49, no. 11, pp. 4177–4193, Nov. 2011.

[11] M. D. Iordache, J. Bioucas-Dias, and A. Plaza, "Sparse unmixing of hyperspectral data," *IEEE Trans. Geosci. Remote Sens.*, vol. 49, no. 6, pp. 2014–2039, Jun. 2011.

[12] M. D. Iordache, J. M. Bioucas-Dias, and A. Plaza, "Total variation spatial regularization for sparse hyperspectral unmixing," *IEEE Trans. Geosci. Remote Sens.*, vol. 50, no. 11, pp. 4484–4502, Nov. 2012.

[13] J. M. P. Nascimento and J. M. Bioucas-Dias, "Hyperspectral unmixing based on mixtures of Dirichlet components," *IEEE Trans. Geosci. Remote Sens.*, vol. 50, no. 3, pp. 863–878, Mar. 2012.

[14] D. D. Lee and H. S. Seung, "Algorithms for non-negative matrix factorization," in *Proc. Adv. Neural Inf. Process. Syst.*, 2001, pp. 556–562.

[15] J. Plaza, A. Plaza, and R. Perez, "On use of small training sets for ANN-based characterization of mixed pixels in hyperspectral," *Pattern Recognit.*, vol. 42, pp. 32–45, 2009.

[16] Y. Su *et al.*, "DAEN: Deep autoencoder networks for hyperspectral unmixing," *IEEE Trans. Geosci. Remote Sens.*, vol. 57, no. 7, pp. 4309–4321, Jul. 2019.

[17] Y. Qian, F. Xiong, Q. Qian, and J. Zhou, "Spectral mixture model inspired network architectures for hyperspectral unmixing," *IEEE Trans. Geosci. Remote Sens.*, vol. 58, no. 10, pp. 7418–7434, Oct. 2020.

[18] Y. Su, A. Marinoni, J. Li, J. Plaza, and P. Gamba, "Stacked nonnegative sparse autoencoders for robust hyperspectral unmixing," *IEEE Geosci. Remote Sens. Lett.*, vol. 15, no. 9, pp. 1427–1431, Sep. 2018.

[19] B. Palsson, M. O. Ulfarsson, and J. R. Sveinsson, "Convolutional autoencoder for spectral-spatial hyperspectral unmixing," *IEEE Trans. Geosci. Remote Sens.,* vol. 59, no. 1, pp. 535–549, Jan. 2021.

[20] Y. Zhou, A. Rangarajan, and P. D. Gader, "A Gaussian mixture model representation of endmember variability in hyperspectral unmixing," *IEEE Trans. Image Process.*, vol. 27, no. 5, pp. 2242–2256, May 2018.

[21] Y. Ma *et al.*, "Hyperspectral unmixing with Gaussian mixture model and low-rank representation," *Remote Sens.,* vol. 11, no. 8, Apr. 2019, Art. no. 911.

[22] Q. Zhu, Y. Zhong, S. Wu, L. Zhang, and D. Li, "Scene classification based on the sparse homogeneous–heterogeneous topic feature model," *IEEE Trans. Geosci. Remote Sens.,* vol. 56, no. 5, pp. 2689–2703, May 2018.

[23] X. Yao, J. Han, G. Cheng, L. Guo, and X. Qian, "Semantic annotation of high-resolution satellite images via weakly supervised learning," *IEEE Trans. Geosci. Remote Sens.*, vol. 54, no. 6, pp. 1–12, Jun. 2016.

[24] W. Wang and H. Qi, "Unsupervised nonlinear unmixing of hyperspectral images using sparsity constrained probabilistic latent semantic analysis," in *Proc. 5th Workshop Hyperspectral Image Signal Process. Evolution Remote Sens.*, Jun. 2013, pp. 1–4.

[25] R. Fernandez-Beltran, A. Plaza, J. Plaza, and F. Pla, "Hyperspectral unmixing based on dual-depth sparse probabilistic latent semantic analysis," *IEEE Trans. Geosci. Remote Sens.*, vol. 56, no. 11, pp. 6344–6360, Nov. 2018.

[26] J. A. G. Jaramago, M. E. Paoletti, J. M. Haut, R. Fernandez-Beltran, A. Plaza, and J. Plaza, "GPU parallel implementation of dual-depth sparse probabilistic latent semantic analysis for hyperspectral unmixing," *IEEE J. Sel. Topics Appl. Earth Observ. Remote Sens.*, vol. 12, no. 9, pp. 3156–3167, Sep. 2019.

[27] O. Eches, N. Dobigeon, and J.-Y. Tourneret, "Enhancing hyperspectral image unmixing with spatial correlations," *IEEE Trans. Geosci. Remote Sens.*, vol. 49, no. 11, pp. 4239–4247, Nov. 2011.

[28] K. Than and T. B. Ho, "Fully sparse topic models," in *Proc. Joint Eur. Conf. Mach. Learn. Princ. Pract. Knowl. Discovery Databases*, 2012, pp. 490–505.

[29] Y. Zhou, E. B. Wetherley, and P. D. Gader, "Unmixing urban hyperspectral imagery using probability distributions to represent endmember variability," *Remote Sens. Environ.*, vol. 246, Sep .2020, Art. no. 111857.

[30] J. C. Bezdek, E. Robert, and F. William, "FCM: The fuzzy C-means clustering algorithm," *Comput. Geosciences*, vol. 10, no. 2/3, pp. 191–203. 1984.

[31] X. Yang, Z. Xie, F. Ling, X. Li, Y. Zhang, and M. Zhong, "Spatio-temporal super-resolution land cover mapping based on fuzzy C-means clustering," *Remote Sens.*, vol. 8, no. 10, Aug. 2018, Art. no. 1212.

[32] D. Blei, A. Ng, and M. Jordan, "Latent Dirichlet allocation," *J. Mach. Learn. Res.*, vol. 3, pp. 993–1022, Jan. 2003.

[33] T. Hofmann, "Unsupervised learning by probabilistic latent semantic analysis," *Mach. Learn.*, vol. 42, no. 1/2, pp. 177–196, Jan. 2001.

[34] D. M. Blei, "Probabilistic topic models," *Commun. ACM*, vol. 55, no. 4, pp. 77–84, Apr. 2012.

[35] Q. Wang, J. Xu, H. Li, and N. Craswell, "Regularized latent semantic indexing," in *Proc. 34th Int. ACM SIGIR Conf. Res. Develop. Inf. Retrieval.*, 2011, pp. 685–694.

[36] C. Wang and D. M. Blei, "Decoupling sparsity and smoothness in the discrete hierarchical Dirichlet process," in *Proc. Adv. Neural Inf. Process. Syst.*, 2009, pp. 1982–1989.

[37] S. Williamson, C. Wang, K. A. Heller, and D. M. Blei, "The IBP compound Dirichlet process and its application to focused topic modeling," in *Proc. 27th Int. Conf. Mach. Learning*, 2010.

[38] W. E. Full, R. Ehrlich, and J. C. Bezdek, "FUZZY QMODEL—A new approach to linear unmixing," *J. Int. Assoc. Math Geol,* vol. 14, pp. 259–270, 1982.

[39] A. Zare and P. Gader, "Piece-wise convex spatial-spectral unmixing of hyperspectral imagery using possibilistic and fuzzy clustering," in *Proc. IEEE Int. Conf. Fuzzy Syst.*, Jun. 2011, pp. 741–746.

[40] S. Chen and D. Zhang, "Robust image segmentation using FCM with spatial constraints based on new kernel-induced distance measure," *IEEE Trans. Syst., Man Cybern.*, vol. 34, no. 4, pp. 1907–1916, Aug. 2004.

[41] R. H. Yuhas, A. F. H. Goetz, and J. W. Boardman, "Discrimination among semi-arid landscape endmembers using the spectral angle mapper (SAM) algorithm," in *Proc. Summaries 3rd Annu. JPL Airborne Geosci. Workshop.*, 1992, vol. 1, pp. 147–149.

[42] K. Canham, A. Schlamm, A. Ziemann, B. Basener, and D. W. Messinger, "Spatially adaptive hyperspectral unmixing," *IEEE Trans. Geosci. Remote Sens.*, vol. 49, no. 11, pp. 4248–4262, Nov. 2011.

[43] Y. Qian, S. Jia, J. Zhou, and A. Robles-Kelly, "Hyperspectral unmixing via sparsity-constrained nonnegative matrix factorization," *IEEE Trans. Geosci. Remote Sens.*, vol. 49, no. 11, pp. 4282–4297, Nov. 2011.

[44] E. M. T. Hendrix, I. Garcia, J. Plaza, G. Martin, and A. Plaza, "A new minimum-volume enclosing algorithm for endmember identification and abundance estimation in hyperspectral data," *IEEE Trans. Geosci. Remote Sens.*, vol. 50, no. 7, pp. 2744–2757, Jul. 2012.
[45] P. O. Hoyer, "Non-negative matrix factorization with sparseness constraints," *J. Mach. Learn. Res.*, vol. 5, pp. 1457–1469, Dec. 2004.
[46] J. Li, J. M. Bioucas-Dias, A. Plaza, and L. Liu, "Robust collaborative nonnegative matrix factorization for hyperspectral unmixing," *IEEE Trans. Geosci. Remote Sens.*, vol. 54, no. 10, pp. 6076–6090, Oct. 2016.
[47] B. Palsson, J. Sigurdsson, J. R. Sveinsson, and M. O. Ulfarsson, "Hyperspectral unmixing using a neural network autoencoder," *IEEE Access*, vol. 6, pp. 25646–25656, 2018.
[48] J. Sigurdsson, M. O. Ulfarsson, J. R. Sveinsson, and J. M. Bioucas-Dias, "Sparse distributed multitemporal hyperspectral unmixing," *IEEE Trans. Geosci. Remote Sens.*, vol. 55, no. 11, pp. 6069–6084, Nov. 2017.
[49] J. Plaza, E. M. T. Hendrix, I. García, G. Martín, and A. Plaza, "On endmember identification in hyperspectral images without pure pixels: A comparison of algorithms," *J. Math. Imag. Vis.*, vol. 42, nos. 2/3, pp. 163–175, Feb. 2012.
[50] J. A. Hartigan and M. A. Wong, "Algorithm AS 136: A K-means clustering algorithm," *J. Roy. Statistcal Soc. C (Appl. Statist.)*., vol. 28, no. 1, pp. 100–108, 1979.
[51] F. Zhu, Y. Wang, B. Fan, S. Xiang, G. Meng, and C. Pan, "Spectral unmixing via data-guided sparsity," *IEEE Trans. Image Process.*, vol. 23, no. 12, pp. 5412–5427, Dec. 2014.
[52] F. Zhu, Y. Wang, S. Xiang, B. Fan, and C. Pan, "Structured sparse method for hyperspectral unmixing," *ISPRS J. Photogrammetry Remote Sens.*, vol. 88, pp. 101–118, Feb. 2014.
[53] Y. Wang, C. Pan, S. Xiang, and F. Zhu, "Robust hyperspectral unmixing with correntropy-based metric," *IEEE Trans. Image Process.*, vol. 24, no. 11, pp. 4027–4040, Nov. 2015.

Qiqi Zhu (Member, IEEE) received the B.S. degree in China University of Mining and Technology, Xuzhou, China, in 2013. She received the Ph.D. degree in photogrammetry and remote sensing from Wuhan University, Wuhan, China, in 2018.

She has been an Associate Professor with the School of Geography and Information Engineering, China University of Geosciences, Wuhan, China, since 2018. She has authored or coauthored more than 30 research papers, including peer-reviewed articles in international journals such as *Remote Sensing of Environment*, *ISPRS Journal of Photogrammetry and Remote Sensing*, and IEEE TRANSACTIONS ON GEOSCIENCE AND REMOTE SENSING. Her research interests include high resolution remote sensing image understanding, geoscience interpretation for multisource remote sensing data, and applications.

Dr. Zhu was a Referee for more than 20 international journals.

Linlin Wang (Graduate Student Member, IEEE) received the B.S. degree in geographic information science from Henan University, Kaifeng, China, in 2019. She is currently working toward the M.S. degree in cartology and geographic information engineering with the School of Geography and Information Engineering, China University of Geosciences, Wuhan, China.

Her major research interests include spectral unmixing for hyperspectral remote sensing imagery, and topic modeling.

Wen Zeng received the B.S. degree in computer software from Huazhong University of Science and Technology, Wuhan, China, in 1991, the M.S. degree in computer software from Jinan University, Guangzhou, China, in 1994, and the Ph.D. degree in cartology and geographic information engineering from China University of Geosciences, Wuhan, China, in 2003.

He has been a Professor with the School of Geography and Information Engineering, China University of Geosciences, Wuhan, China, since 2007. He has authored or coauthored more than 40 research papers, including peer-reviewed articles in international journals such as *International Journal of Geographical Information Science*, and *Annals of the American Association of Geographers, and Cities*. His research interests include data acquisition and modeling for urban geographic information systems, geographic networks optimization, geographic information systems for transportation, and municipal infrastructure management.

Qingfeng Guan received the B.S. degree in geography from East China Normal University, Shanghai, China, in 2000, the M.S. degree in geographic information science and cartography from Chinese Academy of Sciences, Beijing, China, in 2003, and the Ph.D. degree in geographic information science and cartography from University of California, Santa Barbara, CA, USA, in 2008.

He is currently a Full Professor with the School of Geography and Information Engineering, China University of Geosciences, Wuhan, China. His research interests include the application of geospatial big data and high-performance spatial intelligence computation.

Zhen Hu received the B.S. degree in computer science and technology and the Ph.D. degree in cartology and geographic information engineering from China University of Geosciences, Wuhan, China, in 1998 and 2008, respectively.

He has been an Associate Professor of School of Geography and Information Engineering, China University of Geosciences, Wuhan, China, since 2010. He has authored or coauthored more than 10 research papers. His research interests include data acquisition and modeling for urban geographic information systems, geographic networks optimization, geographic information systems for transportation, and municipal infrastructure management.